Electronic Supplementary Material (ESI) for Energy & Environmental Science.

Mechanistic insights into phase transition and metal ex-solution phenomena of $Pr_{0.5}Ba_{0.5}Mn_{0.85}Co_{0.15}O_{3-\delta}$ from simple to layered perovskite under reducing conditions and enhanced catalytic activity

Kyeounghak Kim[1], Sangwook Joo[2], Rui Huang[1], Hyung Jun Kim[1], Guntae Kim[2,*], and Jeong Woo Han[1,*]

[1]*Department of Chemical Engineering, Pohang University of Science and Technology (POSTECH), Pohang, Gyeongbuk 37673, Republic of Korea*

[2]*School of Energy and Chemical Engineering, Ulsan National Institute of Science and Technology (UNIST), Ulsan, 44919, Republic of Korea*

Supplementary information

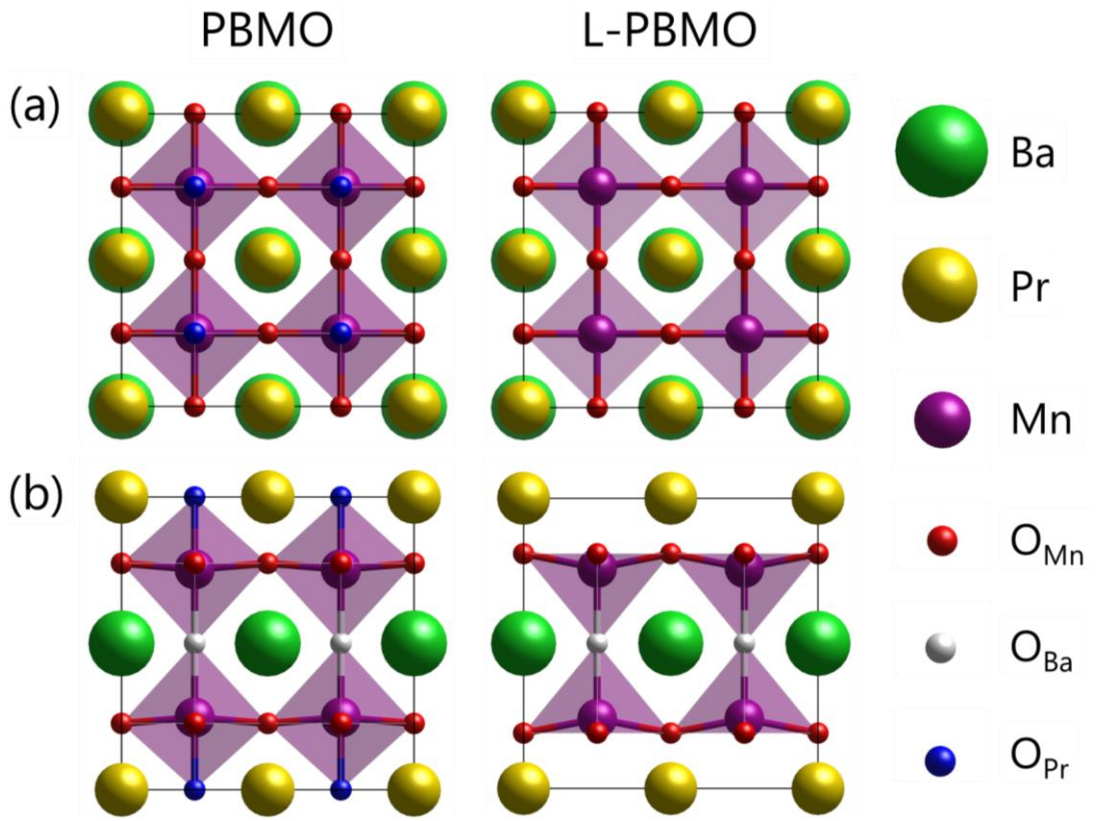

Figure S1. Top (a) and (b) side views of DFT-optimized bulk structures of PBMO and L-PBMO. The red, white, and blue spheres represent possible oxygen vacancy sites at subscript cation-oxygen layer.

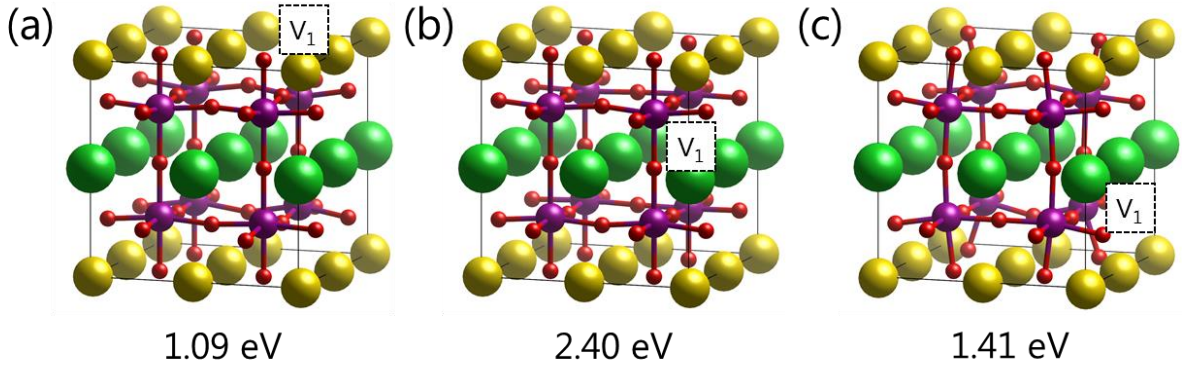

Figure S2. First oxygen vacancy formation sites (V_1) and energies in bulk PBMO. (a), (b), and (c) show the oxygen vacancy sites formed at PrO-, BaO-, and MnO-layer with the corresponding oxygen vacancy formation energies, respectively.

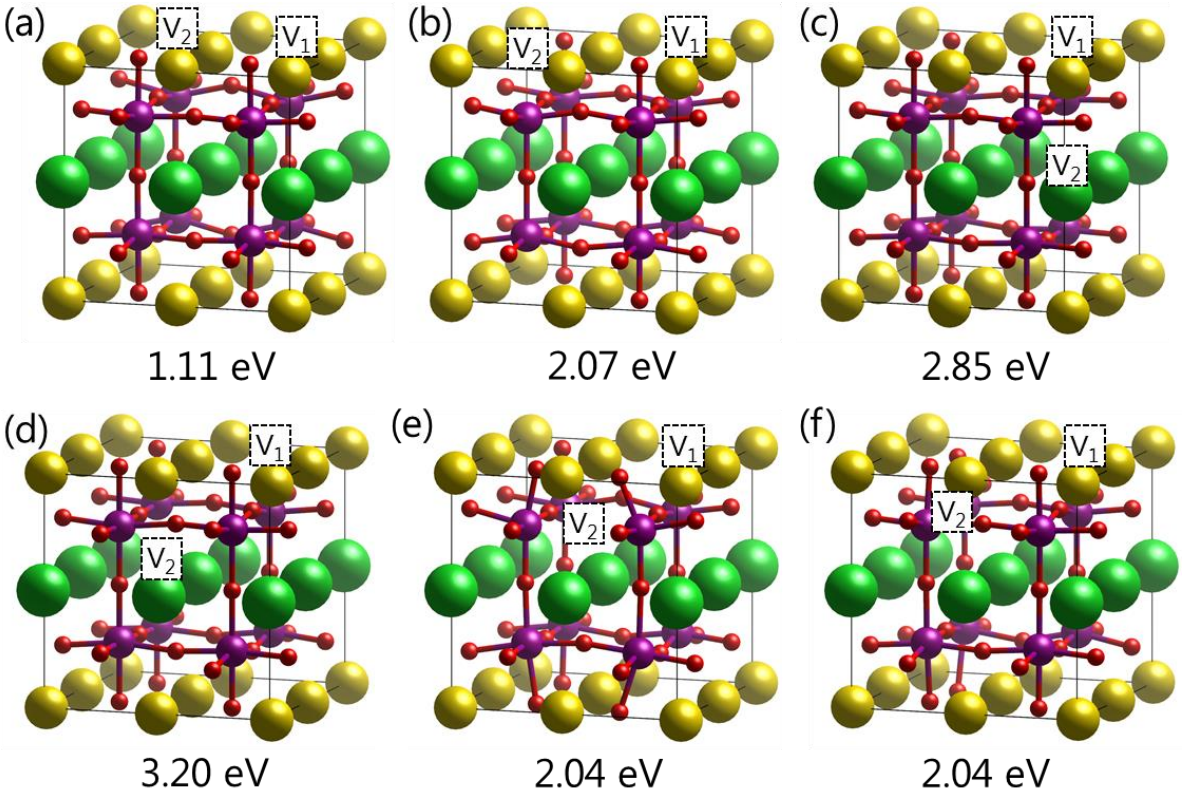

Figure S3. Second oxygen vacancy formation sites (V_2) and energies in bulk PBMO. V_2 in (a and b), (c and d), and (e and f) show the second oxygen vacancy sites formed at PrO-, BaO-, and MnO-layer with the corresponding oxygen vacancy formation energies, respectively.

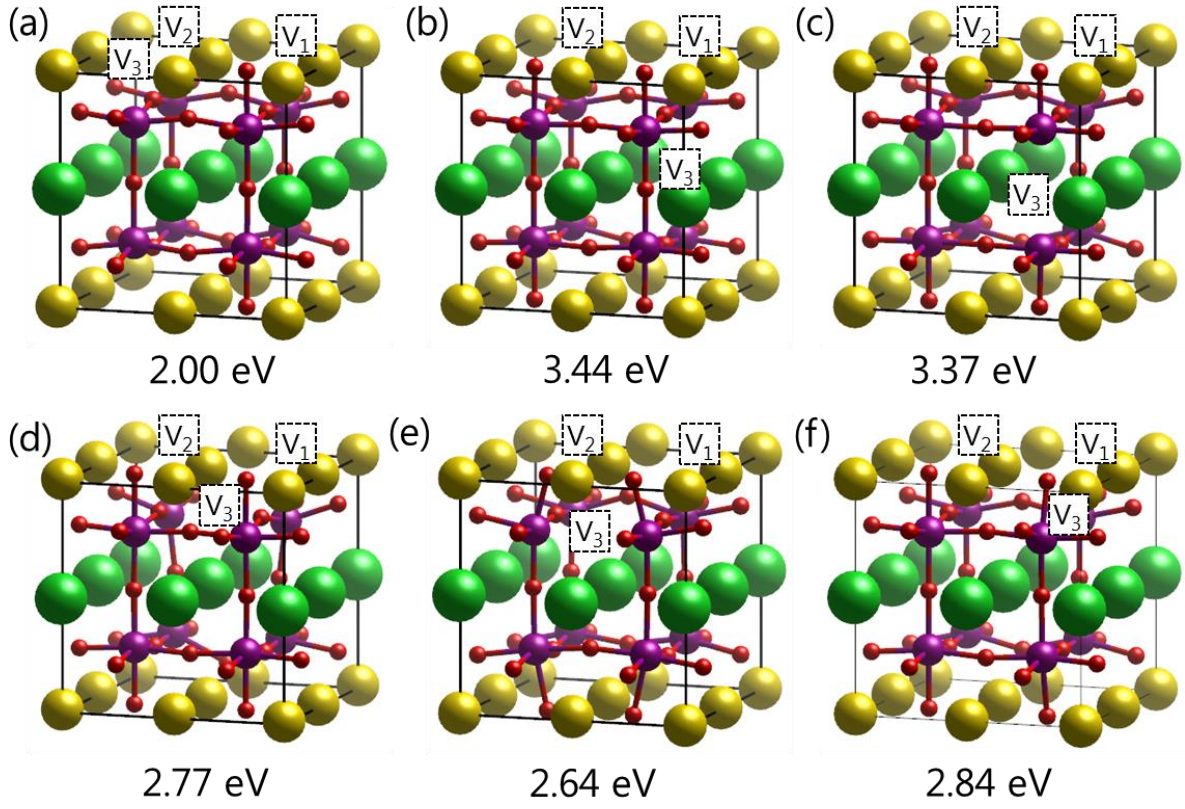

Figure S4. Third oxygen vacancy formation sites (V_3) and energies in bulk PBMO. V_3 in (a), (b and c), and (d ~ f) show the third oxygen vacancy sites formed at PrO-, BaO-, and MnO-layer with the corresponding oxygen vacancy formation energies, respectively.

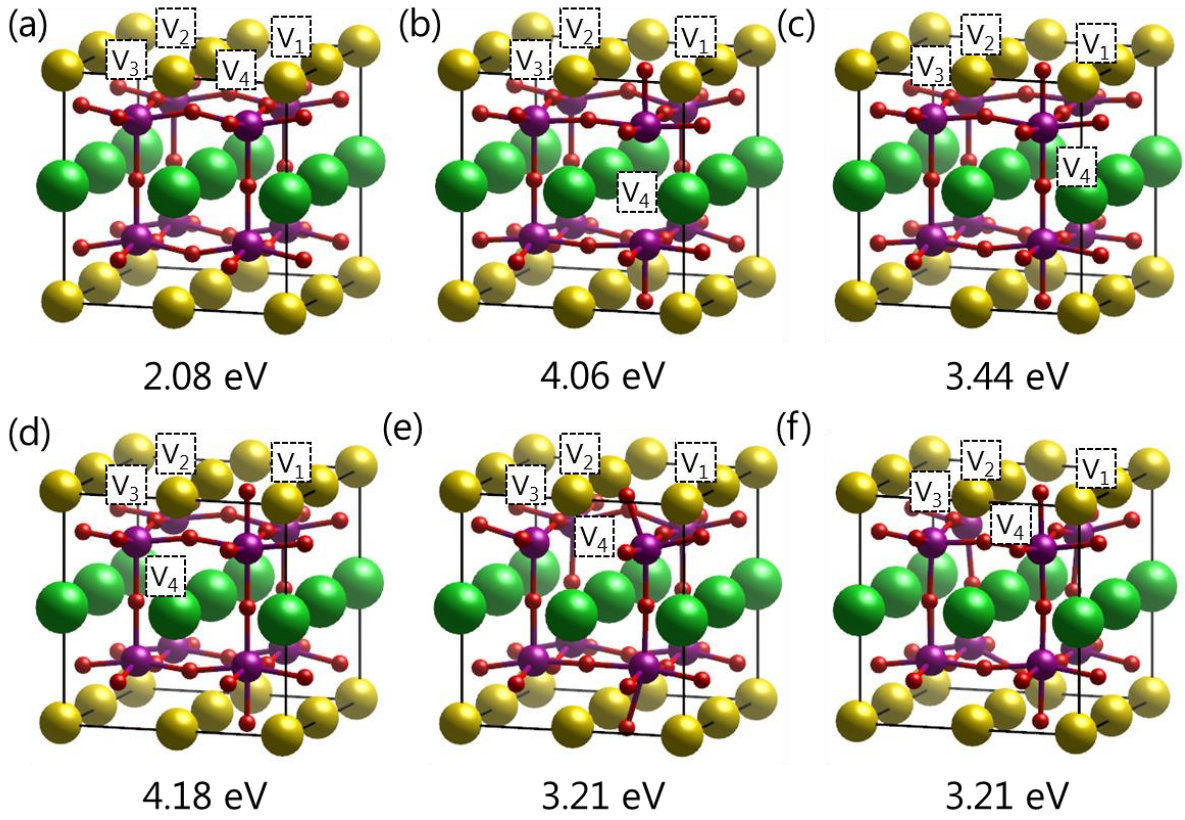

Figure S5. Fourth oxygen vacancy formation sites (V_4) and energies in bulk PBMO. V_4 in (a), (b ~ d), and (e and f) show the fourth oxygen vacancy sites formed at PrO-, BaO-, and MnO-layer with the corresponding oxygen vacancy formation energies, respectively.

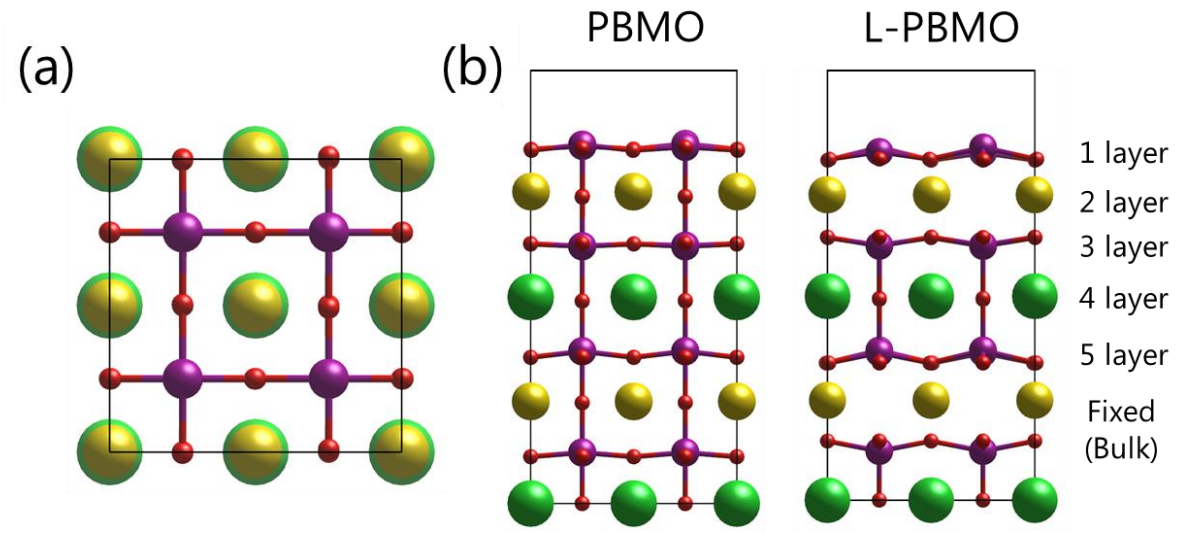

Figure S6. Top (a) and side (b) views for the optimized slab models of PBMO and L-PBMO with possible oxygen vacancy formation sites at each layer.

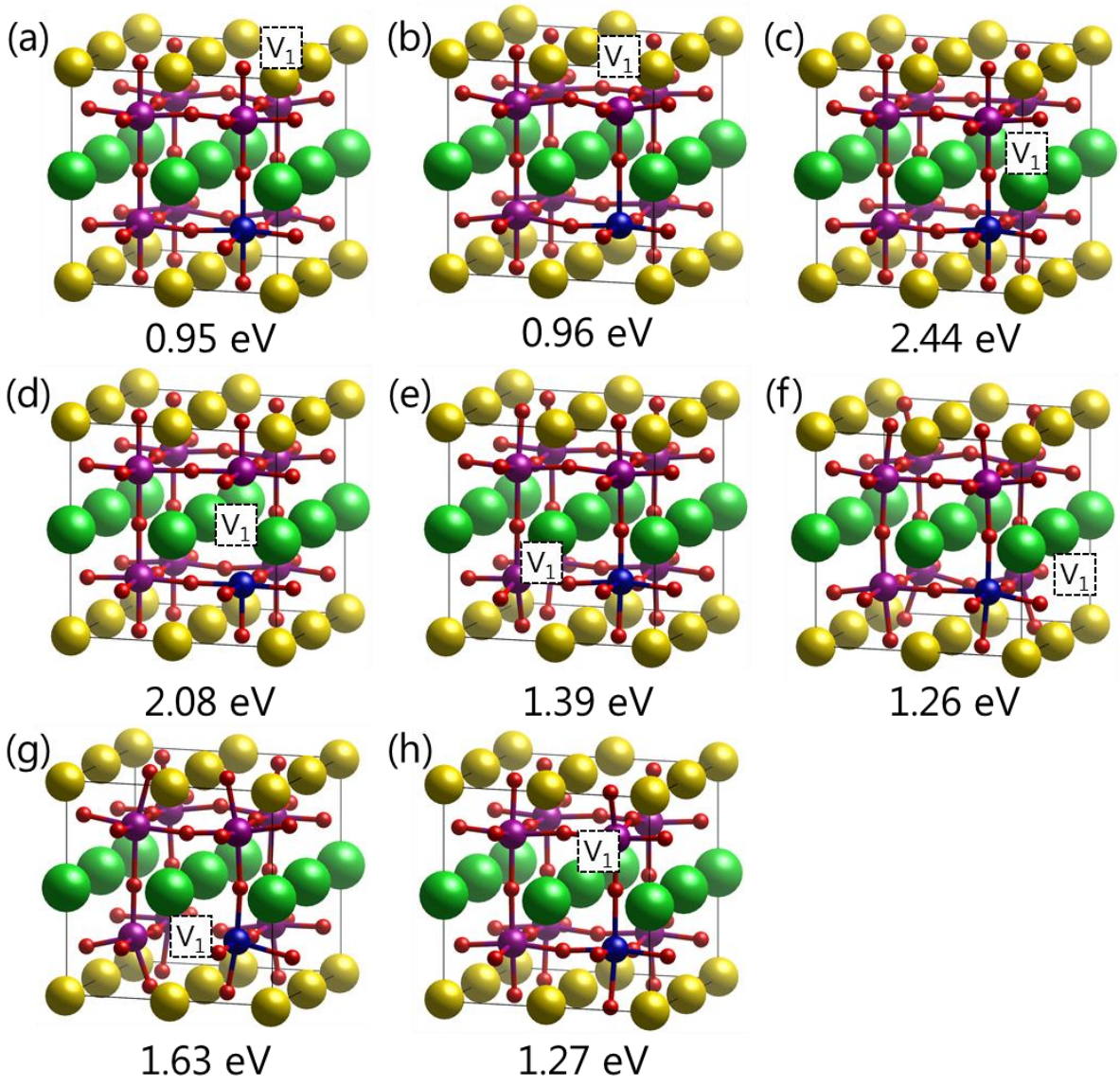

Figure S7. First oxygen vacancy formation sites (V_1) and energies in bulk PBMCO. (a and b), (c and d), and (e ~ h) show the oxygen vacancy sites formed at PrO-, BaO-, and MnO- layer with the corresponding oxygen vacancy formation energies, respectively.

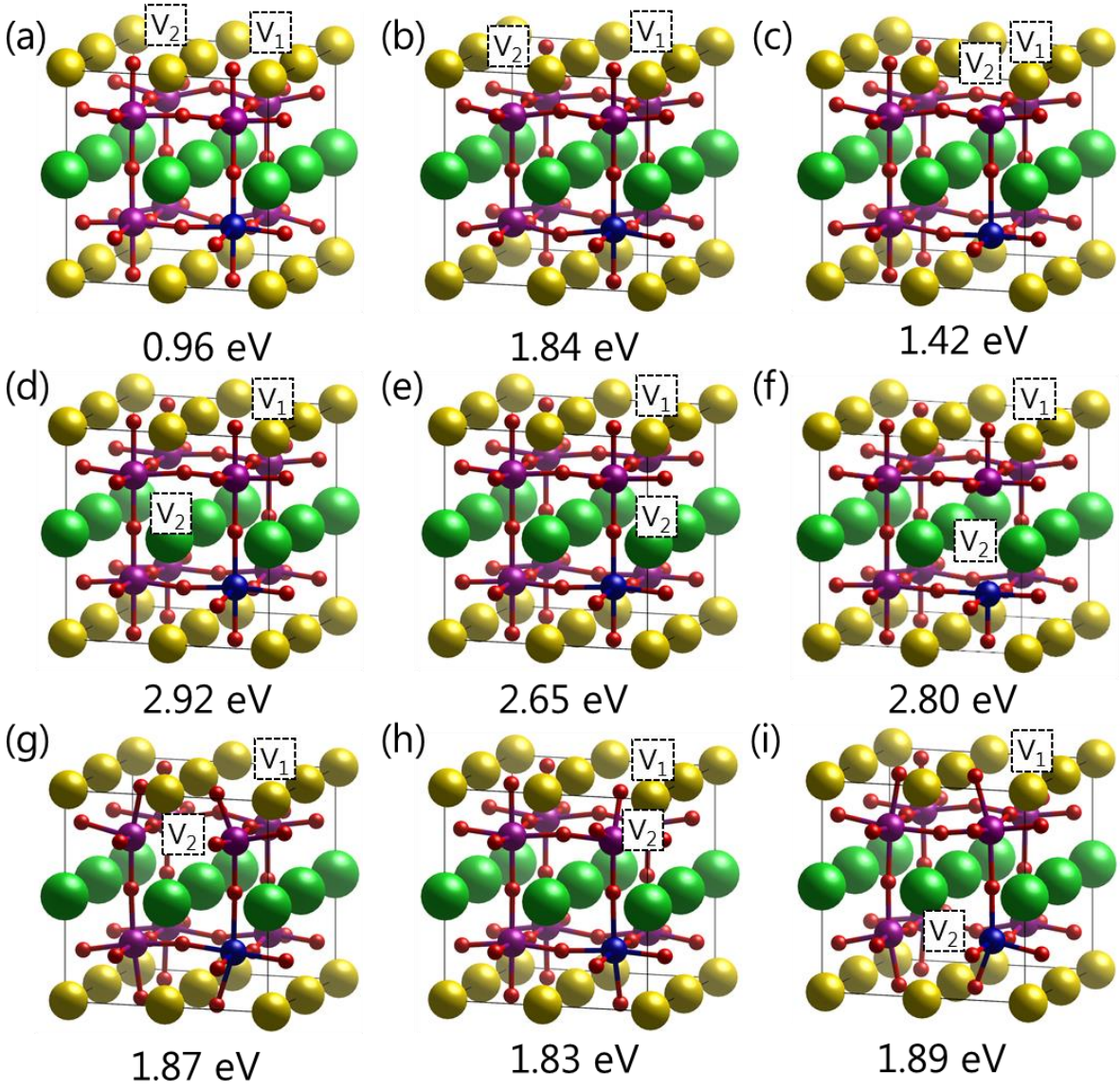

Figure S8. Second oxygen vacancy formation sites (V_2) and energies in bulk PBMCO. V_2 in (a ~ c), (d ~ f), and (g ~ i) show the second oxygen vacancy sites formed at PrO-, BaO-, and MnO- layer with oxygen vacancy formation energies, respectively.

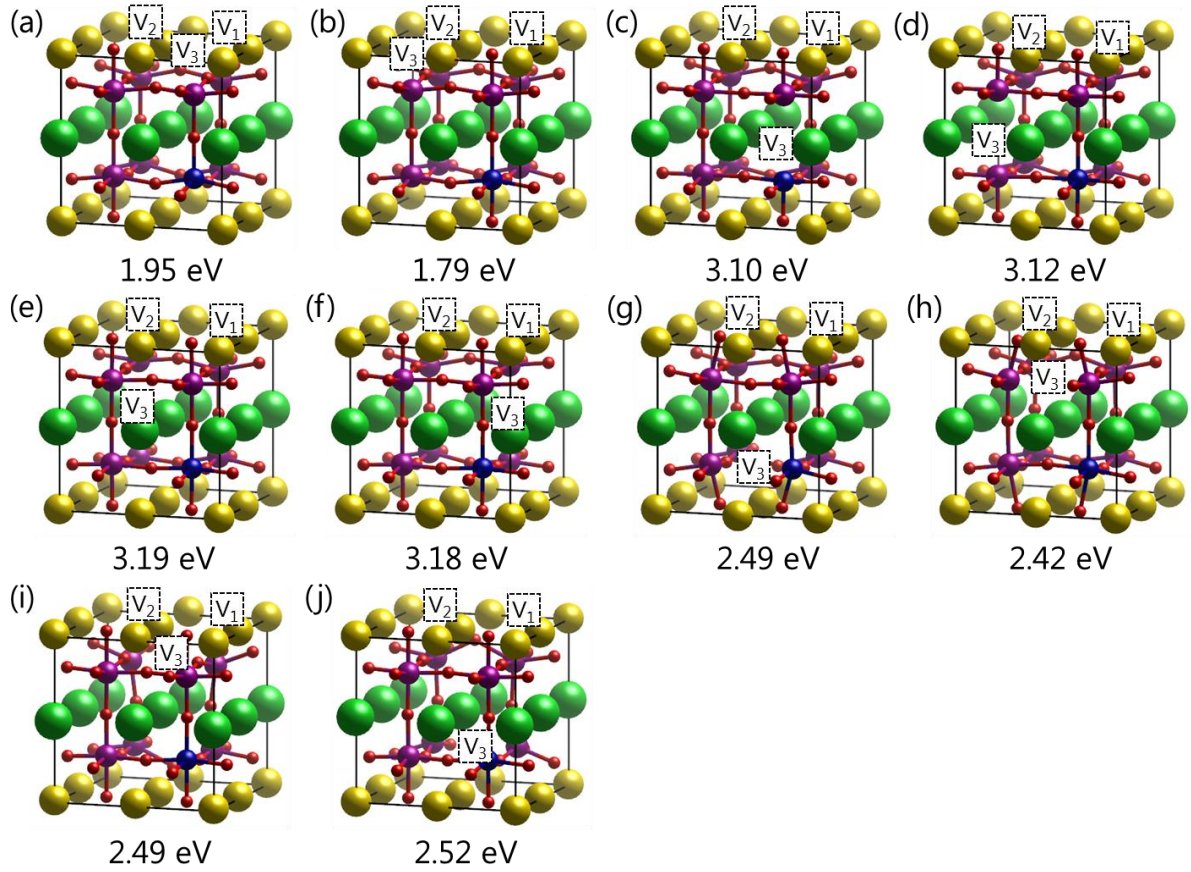

Figure S9. Third oxygen vacancy formation sites (V_3) and energies in bulk PBMCO. V_3 in (a and b), (c ~ f), and (g ~ j) show the third oxygen vacancy sites formed at PrO-, BaO-, and MnO-layer with the corresponding oxygen vacancy formation energies, respectively.

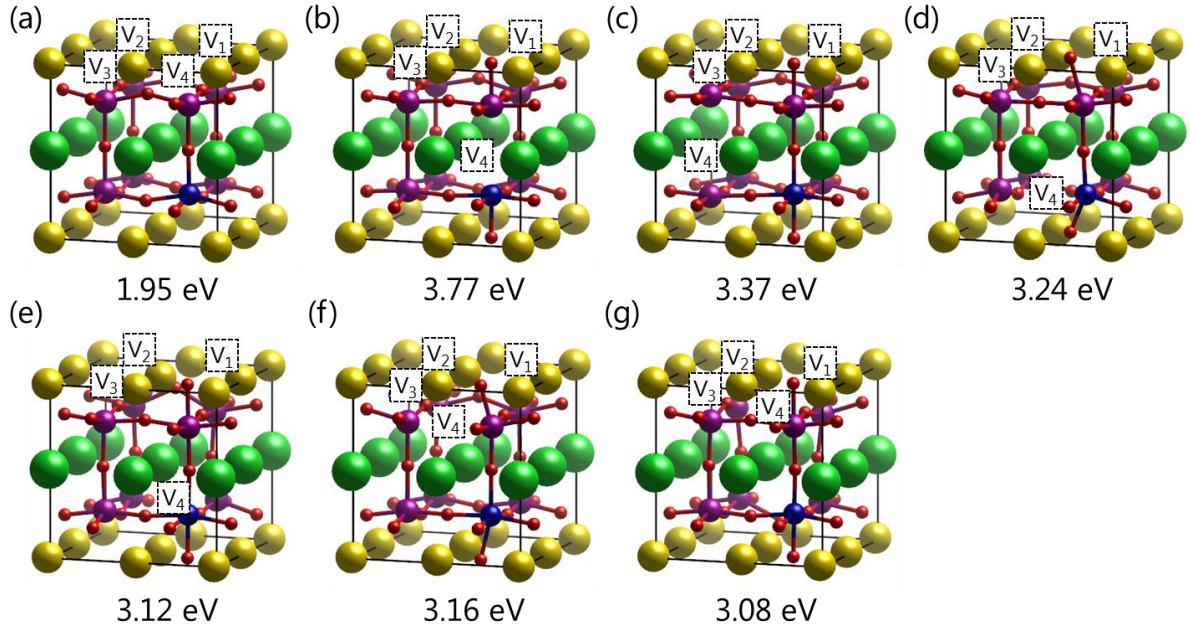

Figure S10. Fourth oxygen vacancy formation sites (V_4) and energies in bulk PBMCO. V_4 in (a), (b and c), and (d ~ g) show the fourth oxygen vacancy sites formed at PrO-, BaO-, and MnO-layer with the corresponding oxygen vacancy formation energies, respectively.

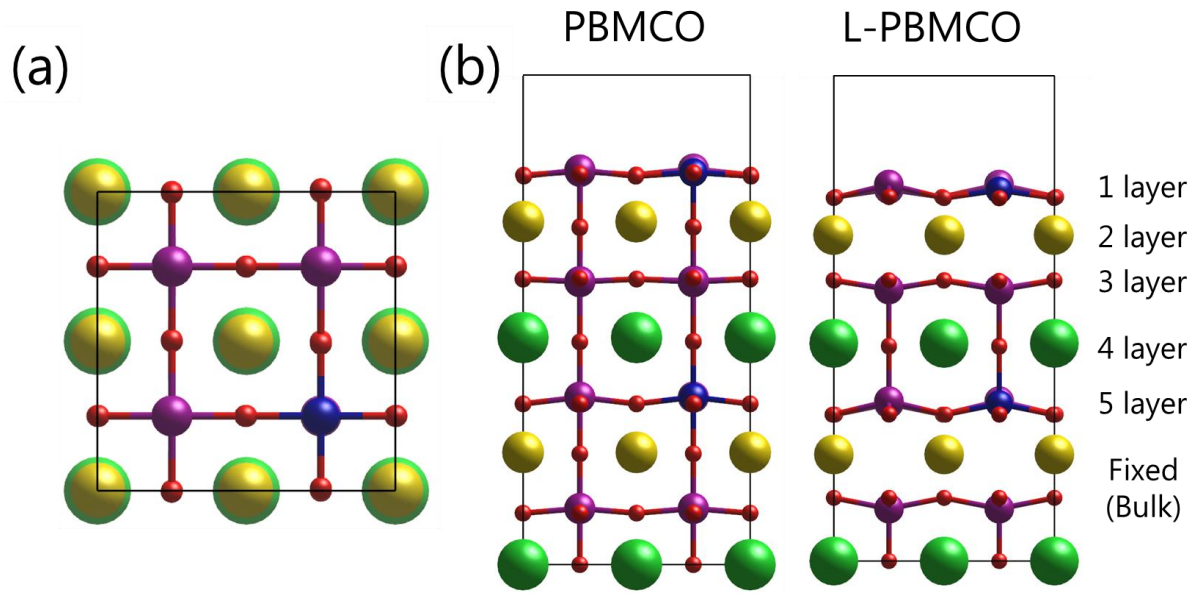

Figure S11. (a) Top and (b) side views of the optimized slab models of PBMCO and L-PBMCO. Note that dopant positions located at 1st layer and 5th layers describe the segregated and as-synthesized dopant states on PBMCO and L-PBMCO, respectively.

Table S1. V_O formation energy [eV] at each layer of bulk and slab models of PBMCO and L-PBMCO (Figure S11).

	PBMCO		L-PBMCO	
	Co at Surface	Co in bulk	Co at Surface	Co in bulk
1 layer	0.73	1.48	2.54	3.68
2 layer	0.42	0.76	-	-
4 layer	1.07	1.51	3.55	3.11
5 layer	0.62	1.31	2.95	3.10

Table S2. Oxide deformation energy of all possible oxide phases of cations that comprise PBMCO. Note that all raw data used in Table S2 are taken by Materials Project database [*Comput. Mater.* **1**, 15010 (2015)].

Oxide phase		Deformation reaction	ΔG_r
$Mn_3O_{4(s)}$	$\xleftrightarrow[H_2]{}$	$3MnO(s) + H_2O(g)$	–167 kJ/mol
$Mn_2O_{3(s)}$	$\xleftrightarrow[H_2]{}$	$2MnO(s) + H_2O(g)$	–197 kJ/mol
$MnO_{(s)}$	$\xleftrightarrow[H_2]{}$	$Mn(s) + H_2O(g)$	–17 kJ/mol
$Co_3O_{4(s)}$	$\xleftrightarrow[H_2]{}$	$3CoO(s) + H_2O(g)$	–215 kJ/mol
$Co_2O_{3(s)}$	$\xleftrightarrow[H_2]{}$	$2CoO(s) + H_2O(g)$	–390 kJ/mol
$CoO_{(s)}$	$\xleftrightarrow[H_2]{}$	$Co(s) + H_2O(g)$	–146 kJ/mol
$BaO_{2(s)}$	$\xleftrightarrow[H_2]{}$	$BaO(s) + H_2O(g)$	–322 kJ/mol
$BaO_{(s)}$	$\xleftrightarrow[H_2]{}$	$Ba(s) + H_2O(g)$	144 kJ/mol
$Pr_5O_{9(s)}$	$\xleftrightarrow[H_2]{}$	$5PrO(s) + 4H_2O(g)$	4 kJ/mol
$Pr_2O_{3(s)}$	$\xleftrightarrow[H_2]{}$	$2PrO(s) + H_2O(g)$	227 kJ/mol
$PrO_{(s)}$	$\xleftrightarrow[H_2]{}$	$Pr(s) + H_2O(g)$	188 kJ/mol

Table S3. Total energies that correspond to the optimized structures of PBMCO (Figure S12 ~ S14) and L-PBMCO (Figure S15 ~ S17).

		CON1	CON2	CON3	CON4	CON5	CON6
PBMCO	Clean	-572.603	-572.630	-572.596	-572.579	-572.516	-572.864
	V1	-567.363	-566.961	-566.154	-567.000	-567.066	-567.133
	V2	-567.017	-567.314	-566.766	-567.327	-567.328	-567.443
	V3	-567.339	-567.223	-567.482	-566.667	-566.690	-566.130
	V4	-566.627	-566.369	-566.734	-565.551	-566.369	-565.968
	V5	-566.556		-566.553	-567.236	-567.165	-566.708
	V6	-567.105		-565.563		-566.477	-566.107
L-PBMCO	Clean	-524.565	-524.580	-524.501	-524.469	-524.525	-524.477
	V1	-517.383	-517.180	-517.134	-517.018	-516.967	-516.920
	V2	-517.060	-516.711	-516.686	-517.083	-516.637	-516.956
	V3	-516.811	-516.094	-516.922	-516.622	-516.680	-516.488
	V4	-516.672		-516.671	-516.614	-516.612	
	V5	-516.703		-516.455	-516.481	-516.659	
	V6	-516.727		-516.105		-516.321	

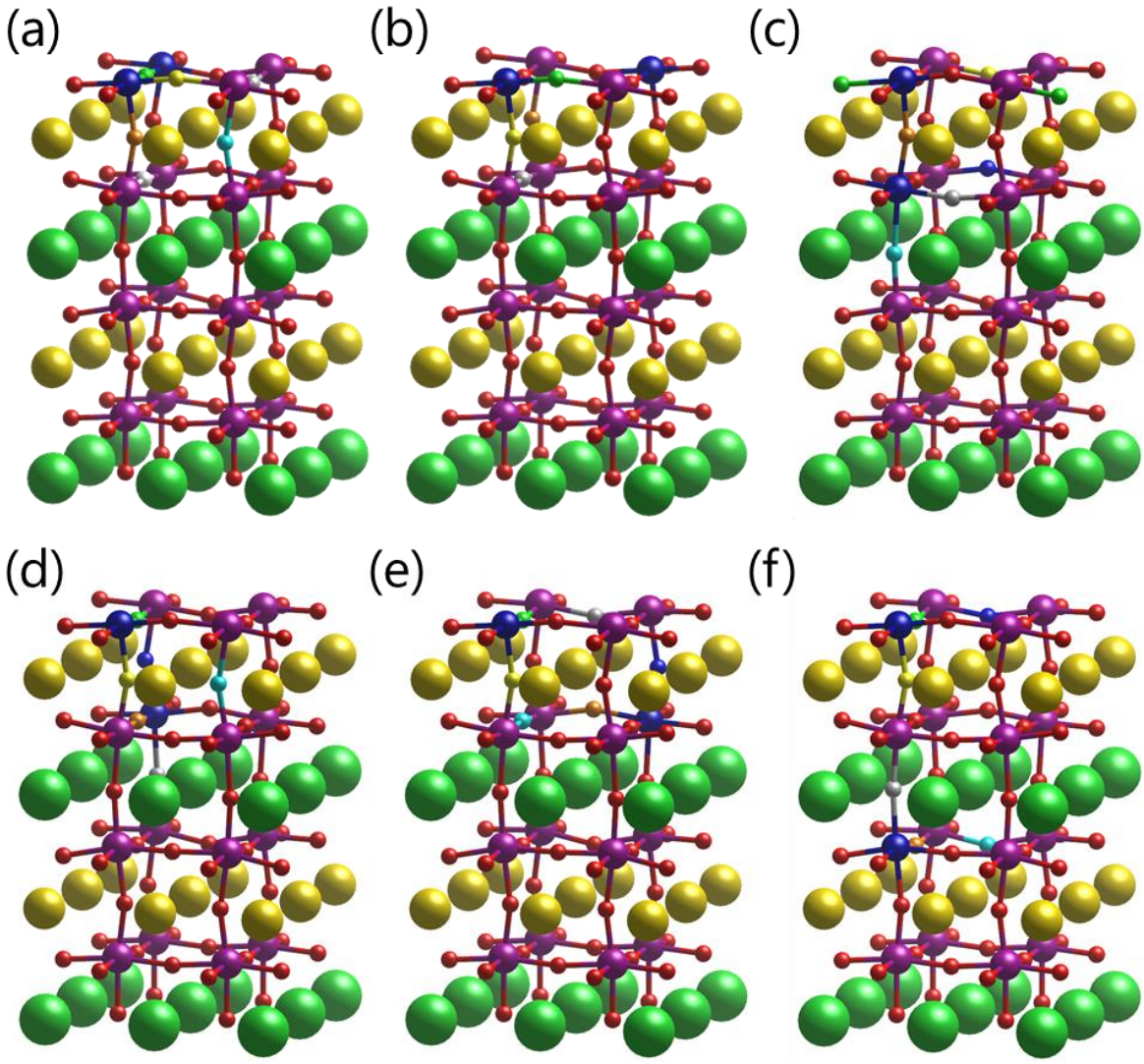

Figure S12. (a ~ f) Possible atomic configurations of two Co doped PBMCO. (a, b) are the structures with both Co located at top surface, (c ~ e) are the structures with one Co located at top surface and another Co located at the second MnO-layer, and (f) is the structure with one Co located at top surface and another Co located at the third MnO-layer.

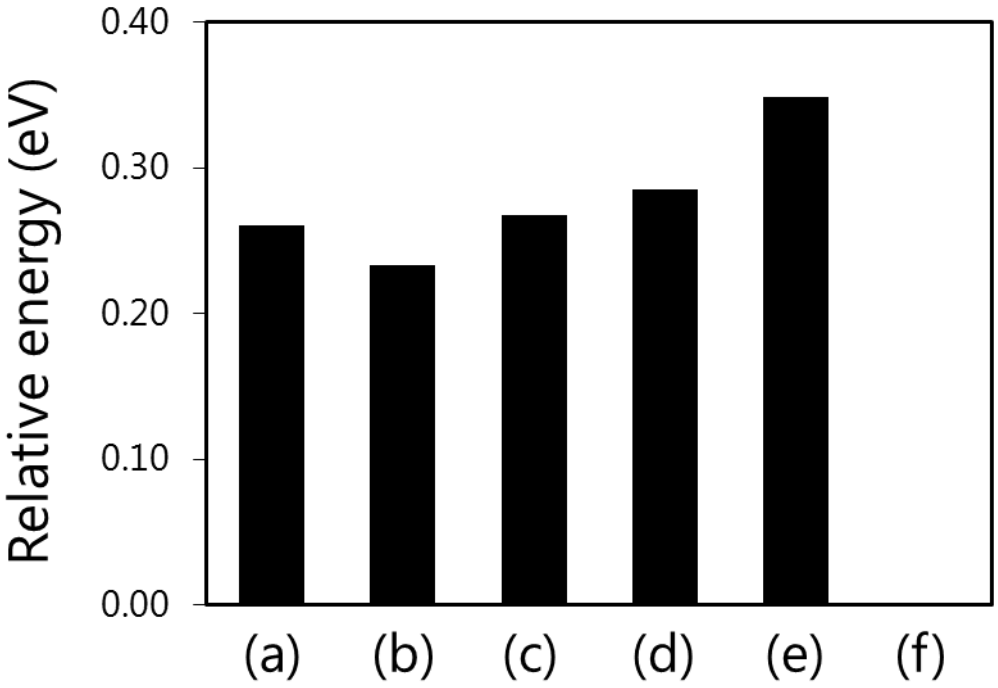

Figure S13. Relative total energies of two Co doped PBMCO referenced to the most stable (f) shown in Figure S12.

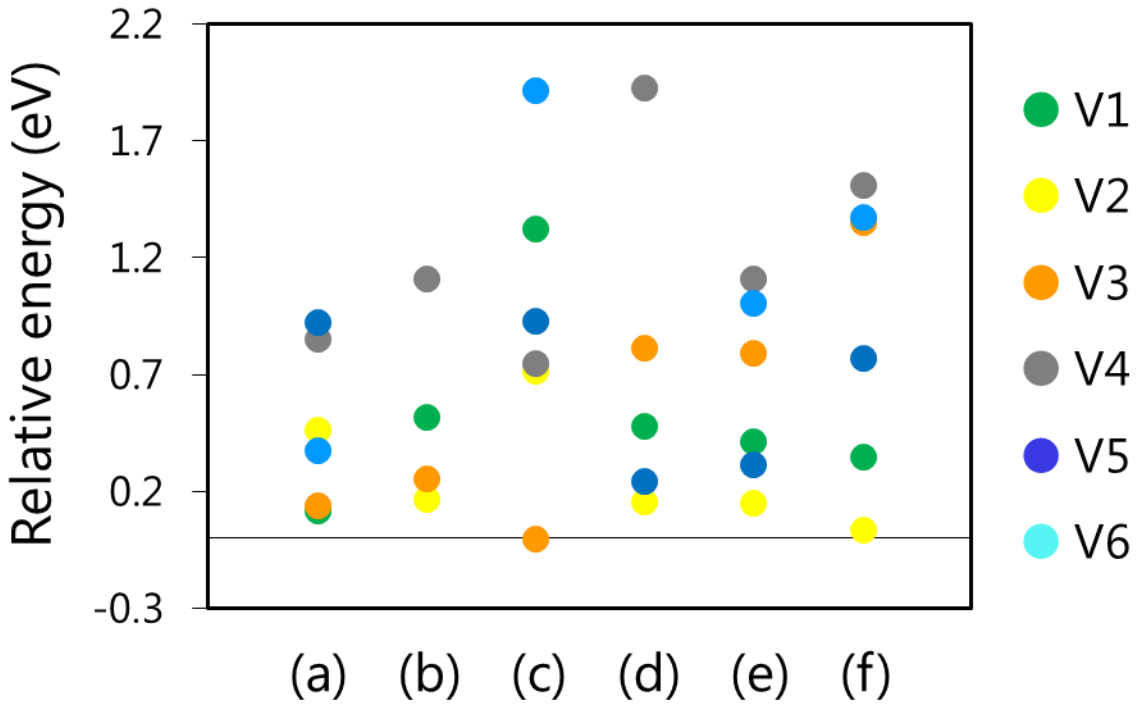

Figure S14. Relative total energies of two Co doped PBMCO with an oxygen vacancy. The colors of V_x correspond to those in Figure S12 at oxygen sites at each configuration.

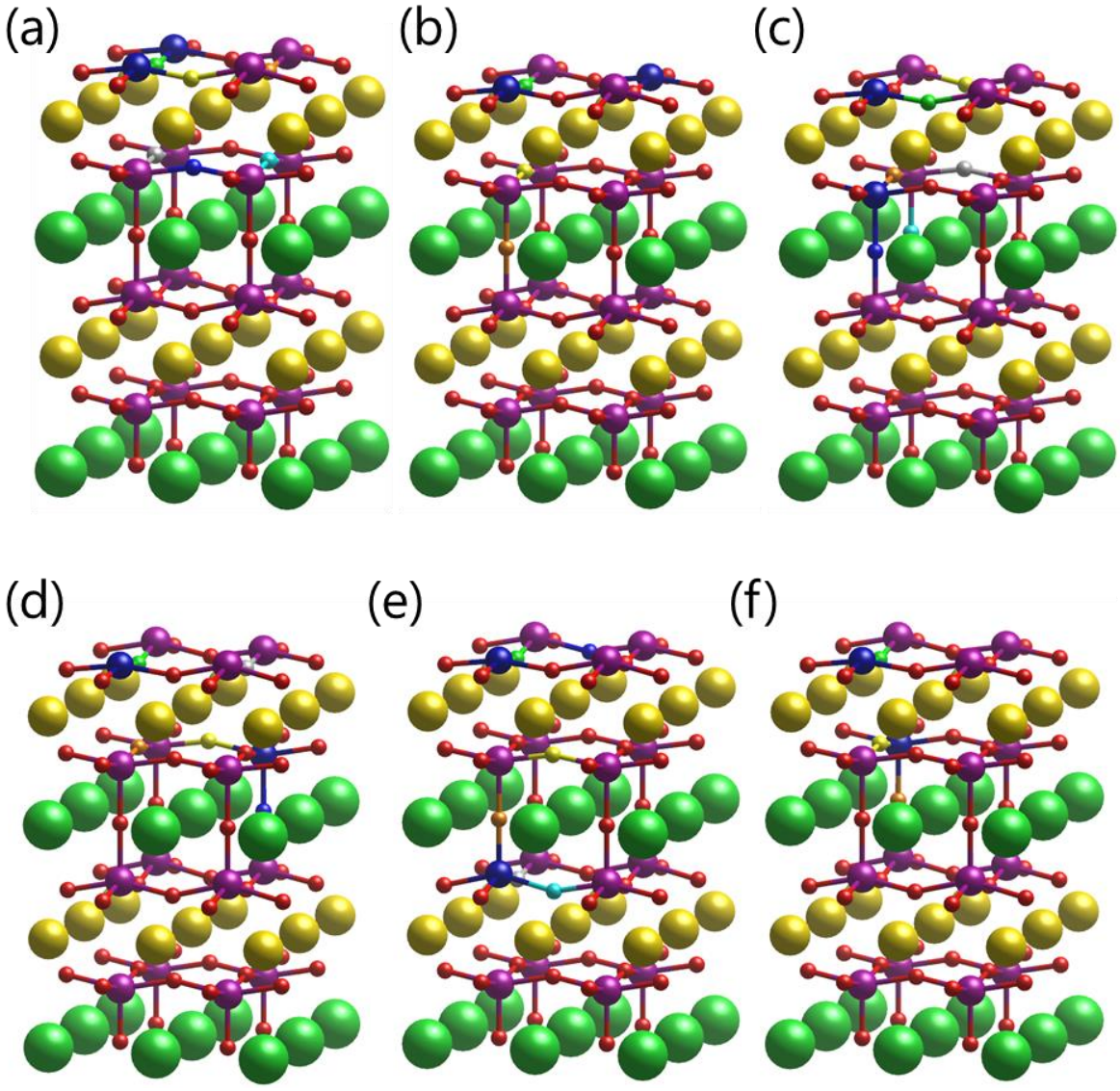

Figure S15. (a ~ f) Possible atomic configurations of two Co doped L-PBMCO. (a, b) are the structures with both Co located at top surface, (c ~ e) are the structures with one Co located at top surface and another Co located at the second MnO-layer, and (f) is the structure with one Co located at top surface and another Co located at the third MnO-layer.

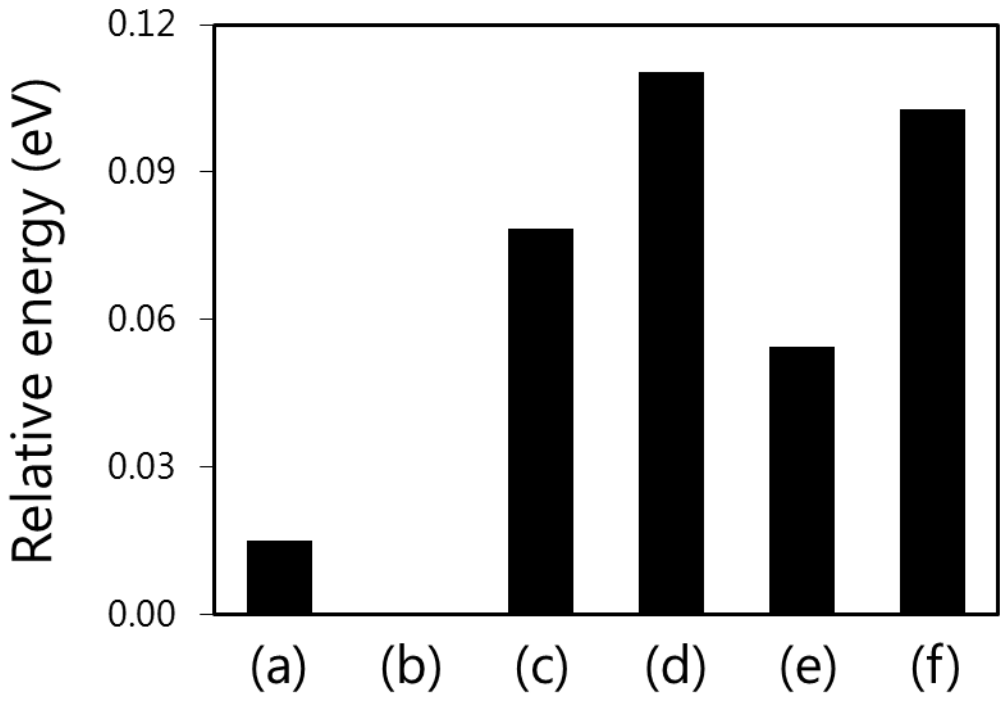

Figure S16. Relative total energies of two Co doped L-PBMCO referenced to the most stable (b) shown in Figure S15.

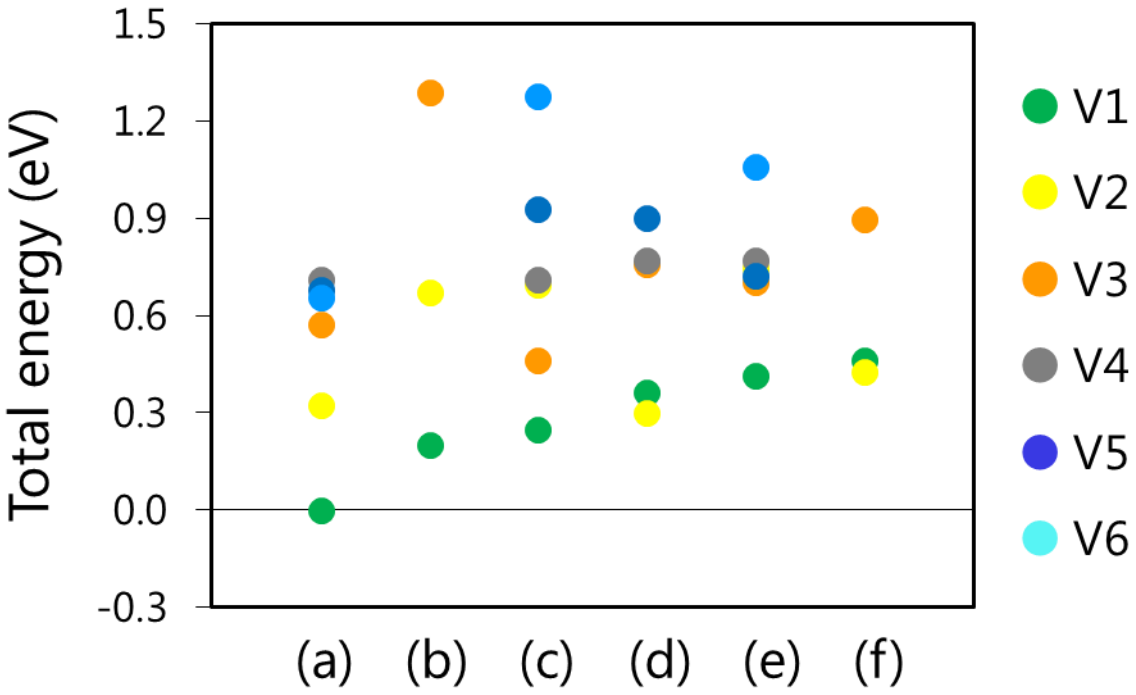

Figure S17. Relative total energies of two Co doped L-PBMCO with an oxygen vacancy. The colors of V_x correspond to those in Figure S15 at oxygen sites at each configuration.

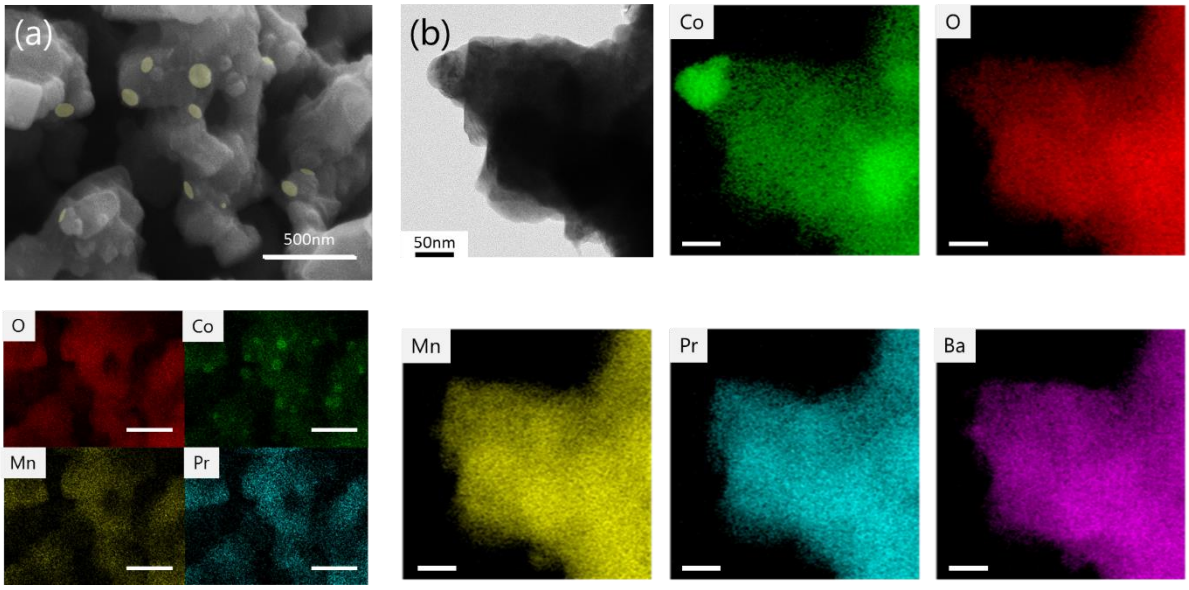

Figure S18. (a) SEM, (b) TEM images and EDS mapping of each element; O (red), Co (green), Mn (yellow), Pr (cyan) and Ba(pink) for Co@L-PBMCO after CO oxidation. Ex-solved Co nanoparticles in (a) are highlighted as yellow.

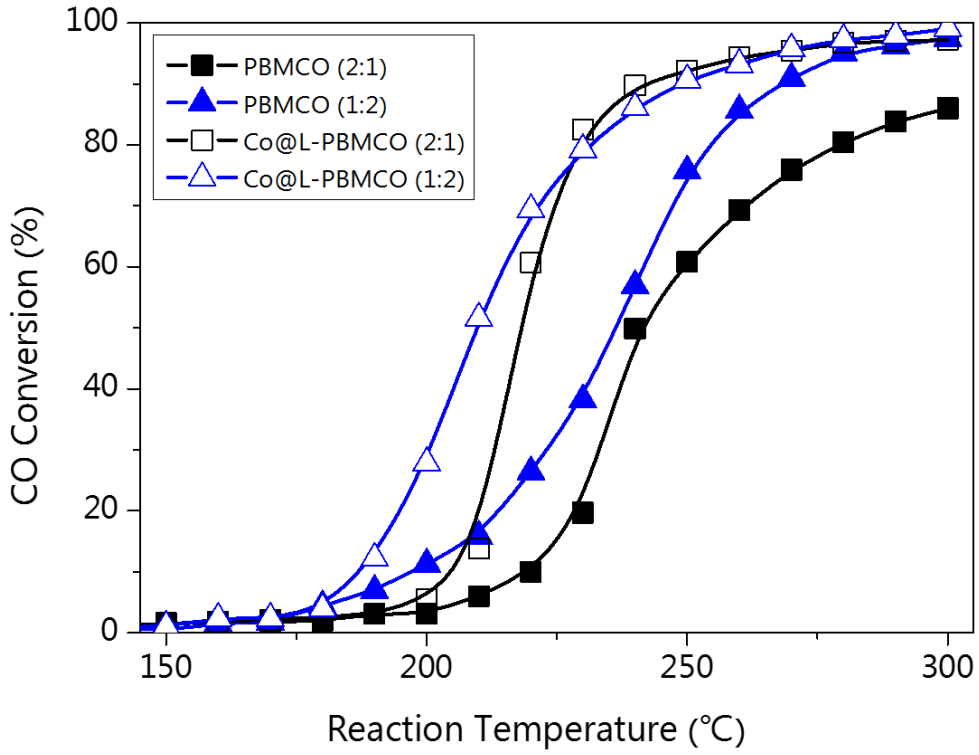

Figure S19. Catalytic activity curves for CO conversion ratio with respect to temperature before (PBMCO) and after Co ex-solution (Co@L-PBMCO) under CO/O_2 ratio of 1:2. Catalytic activity curves for CO conversion under CO/O_2 ratio of 2:1 are also shown for the comparison.

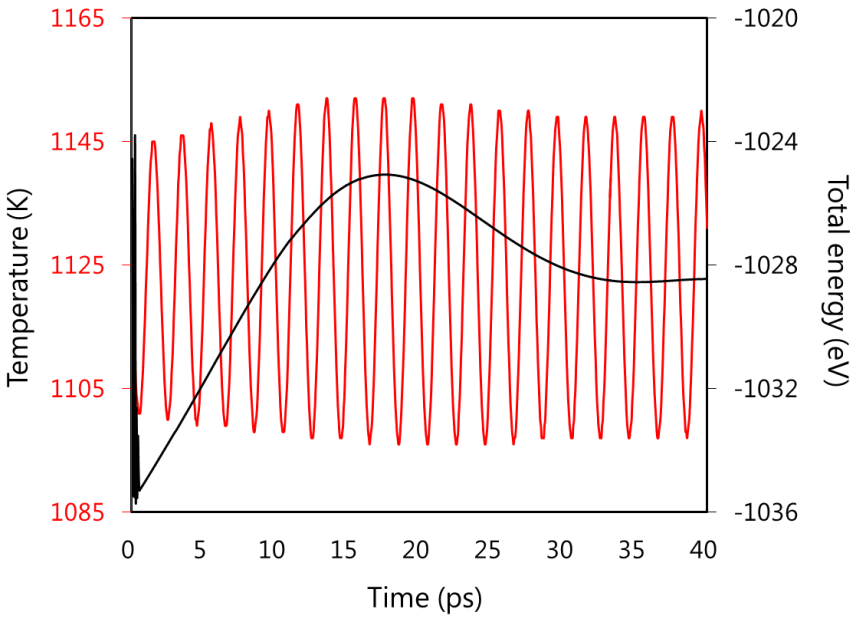

Figure S20. Temperature and total energy of Co@L-PBMCO as a function of *ab initio* molecular dynamics (AIMD) simulation time.

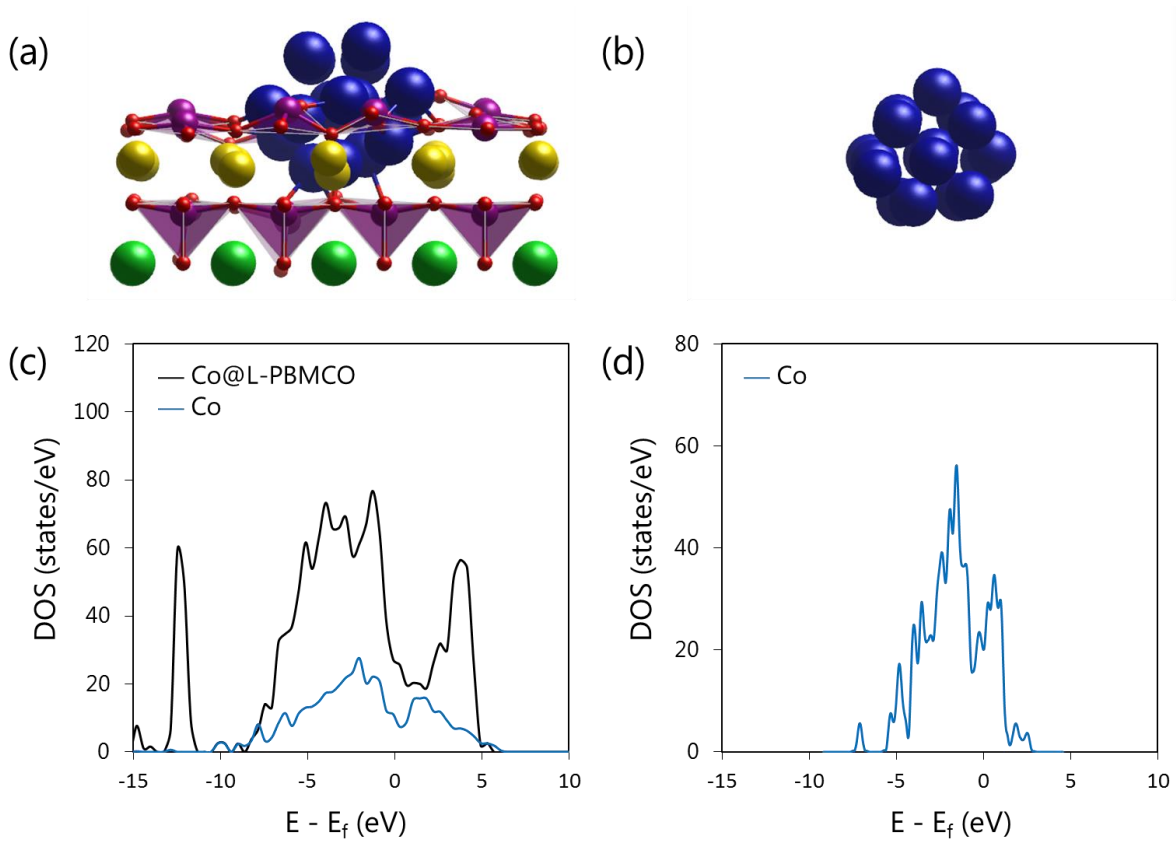

Figure S21. Optimized structures and total density of states (states/eV) of (a and c) Co@L-PBMCO and (b and d) Co nanoparticle. The Fermi level E_f is shifted to zero. The blue line in Figure S21c is the total density of states of ex-solved Co atoms in (a) Co@L-PBMCO.

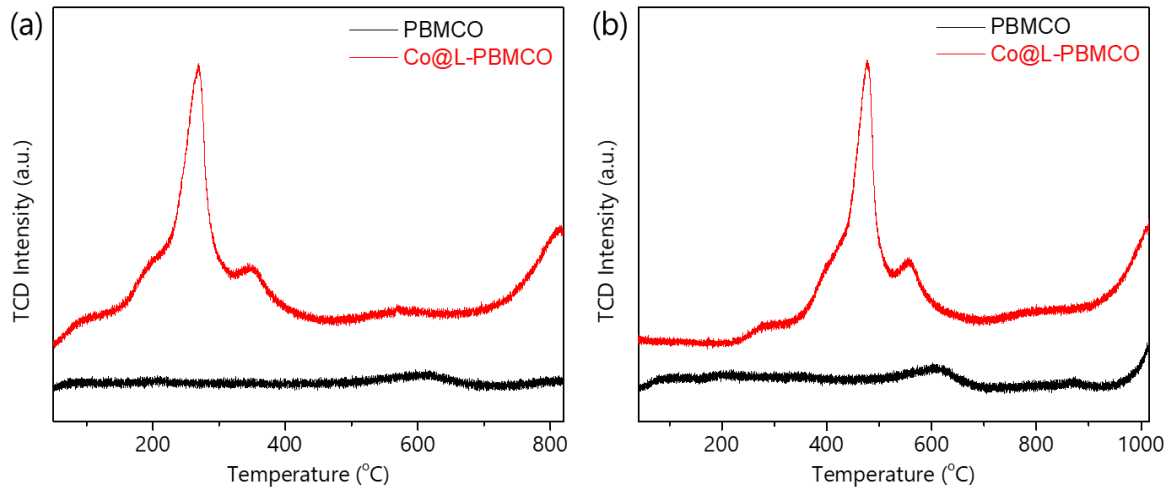

Figure S22. (a) CO-TPD and (b) O_2-TPD curve before (PBMCO, black) and after Co exsolution (Co@L-PBMCO, red).

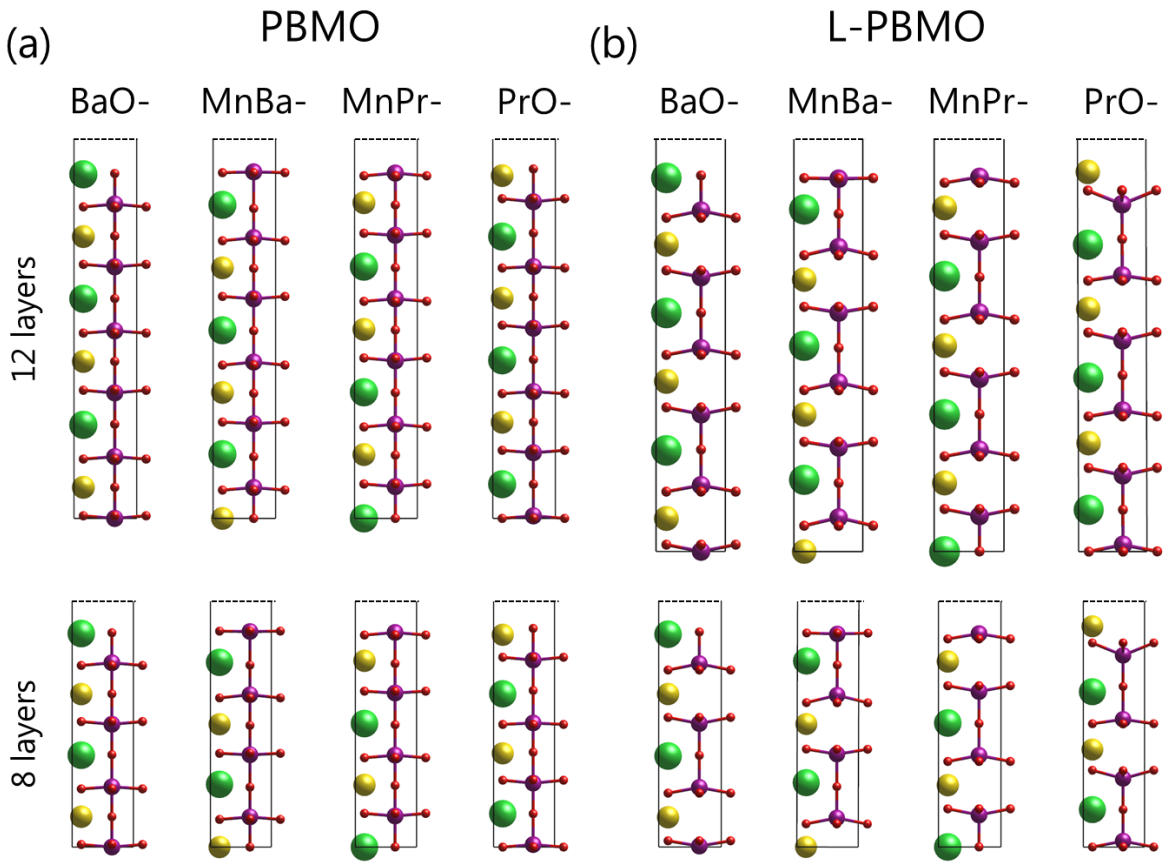

Figure S23. Top and side views of optimized surface structures of 8 and 12 layers of (a) PBMO and (b) L-PBMO.

Table S4. DFT-calculated surface energies [eV/Å^2] of 8 and 12 layers slab models with possible surface terminations.

	8 layers		12 layers	
	PBMO	L-PBMO	PBMO	L-PBMO
BaO	0.063	0.041	0.068	0.039
PrO	0.098	0.177	0.109	0.175
MnBa	0.124	0.175	0.133	0.173
MnPr	0.064	0.042	0.068	0.040